Scientific Research Publishing

Wireless Engineering and Technology, 2018, 9, 66-78
http://www.scirp.org/journal/wet
ISSN Online: 2152-2308
ISSN Print: 2152-2294

Aperture Efficiency Study of Square Reflect Array Antennas

Javad Nourinia, Changiz Ghobadi, Bahman Mohammadi, Farzad Alizadeh

Department of Electrical Engineering, Urmia University, Urmia, Iran
Email: j.nourinia@urmia.ac.ir

How to cite this paper: Nourinia, J., Ghobadi, C., Mohammadi, B. and Alizadeh, F. (2018) Aperture Efficiency Study of Square Reflect Array Antennas. *Wireless Engineering and Technology*, **9**, 66-78.
https://doi.org/10.4236/wet.2018.93006

Received: April 23, 2018
Accepted: July 17, 2018
Published: July 20, 2018

Abstract

This paper presents a detailed study of square reflect array (RA) antenna aperture efficiency (η_a). Effects of quantization-phase and limited phase-range errors on radiation pattern, half-power beam width (HPBW) and η_a for different feed locations are investigated. Results show an increase in side-lobe levels (SLLs) and a slightly reduction in η_a with quantization-phase augmentation or element phase-range reduction, however, the effects on HPBW are negligible. Nevertheless, the degradation in η_a is negligible when the quantization-phase is lower than 30˚ or phase-range is more than 300˚. Parametric studies have been carried out to provide design guidelines to maximize η_a. It is perceived that the offset-angle plays an important role to determine η_a, especially for feed with narrow beam width.

Keywords

Aperture Efficiency, Limited Phase-Range Error, Quantization-Phase Error, Reflect array Antennas, Square Aperture

1. Introduction

Reflect array (RA) antenna is comprised of a quasi-periodic set of unit elements mostly set in a regular lattice to emulate a specific phase-front transformation [1] [2] [3]. RAs have many technological benefits compared to parabolic reflectors [4], like ameliorated cross-polarization performance due to the polarization sensitive elements, feed blockage reduction with center-fed offset-beam structure, simply folded mechanism for packaging and transportation by division into small segments, keeping the price low with easy manufacturing process for shaped-beam RAs.

Considering the electrically large size of the RAs, composed of many elements with small size lower than a wavelength, a full-wave simulation requires a consi-

derably high computational time and huge resource. Similar to the look of the standard reflectors, η_a and radiation properties need to be predicted in initial RA design procedure to judge the antenna performances. A design parameter r_f (is the focal length to aperture side length ratio) should be correctly selected. Larger r_f value results in smaller phase sensitivity to frequency variation and typically enhances radiation performance in terms of cross-polarization level, gain bandwidth, and scan capability. On the other hand, it increases feed size and overall profile of RA antenna, therefore, it demands more mechanical effort to hold the antenna exactly in place [4]. A smaller r_f increases variation of spatial phase delays and causes large incident angles for edge elements.

The main objective of this paper is to study aperture efficiency of a square planar space-fed system. In practice, the phase of each RA element is chosen to resemble the nearest quantization phase. Besides, some phasing elements have a phase-range lower than 360˚. An investigation is presented to survey these errors on side-lobe levels (SLLs), half-power beam widths (HPBWs) and η_a of RAs. By plotting η_a versus configuration parameters, an economical and comparatively correct approximated design procedure ought to be introduced. Comparison between the center- and offset-fed square RAs for different feed locations is given. Square apertures are suitable for development of small spacecrafts based on the Cube Sat standard (3U, equal to 30 cm), which has grown considerably in recent years for low-cost space missions [5] [6].

2. Aperture Efficiency Analysis

Figure 1 shows a typical configuration of a square RA system consist of an array of radiating elements and a feeding source. As demonstrated in Figure 1, four sets of coordinate systems are usually employed to analysis an RA. The subscript f points out the feed coordinates where $\boldsymbol{r}_f$ is the location of feed phase center. In Figure 2 the feed beam direction (FBD) is marked by $P_o(x_o, y_o, 0)$ where the maximum radiation of the feed horn is directed. The θ_o and θ_e are offset-angle of feed source and incidence-angle of mn^{th} element, respectively. The system configuration parameters are listed in Table 1. In Figure 3 Σ points to the spherical surface centered at feed phase center. A shows the RA aperture that is specified by the aperture boundary, and surface σ shares a similar angle with A and Σ [7].

Table 1. The configuration parameters.

Parameter	Quantity
Feed location	$F(0, -r_f\sin\theta_o, r_f\cos\theta_o)$
Feed beam direction (FBD)	$P_o(x_o, y_o, 0)$
Element location	$P(x_{mn}, y_{mn}, 0)$
Location vector from feed to FBD	$\boldsymbol{r}_o = \boldsymbol{FP}_o$
Location vector from feed to the element	$\boldsymbol{r} = \boldsymbol{FP}$
Distance of element and FBD	$s = \lvert\boldsymbol{PP}_o\rvert$

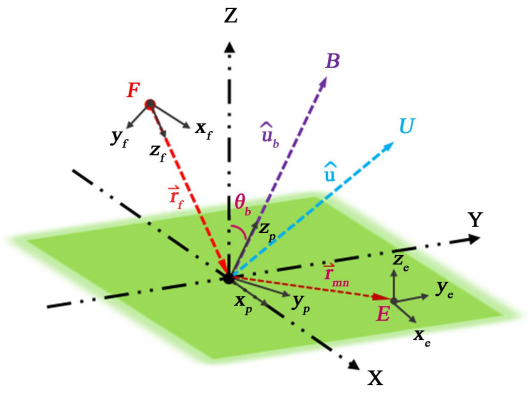

Figure 1. The coordinate systems of a typical reflect array antenna.

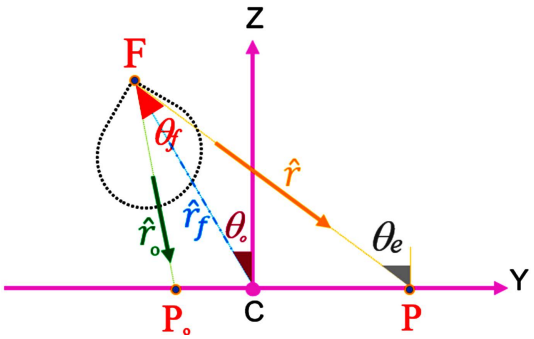

Figure 2. Configuration parameters of a typical reflect array antenna.

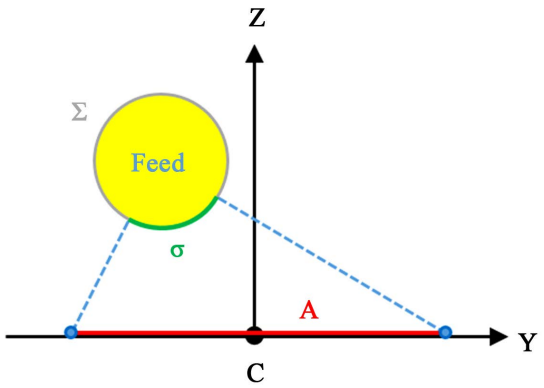

Figure 3. Spherical geometry of a typical reflect array antenna.

The η_a of the whole RA is presented by the product of several sub-efficiency factors [8] [9]:

$$\eta_a = \eta_{spill} \times \eta_{ph} \times \eta_t \times \eta_b \times \eta_x \times \eta_e \times \eta_{et} \times \eta_o . \quad (1)$$

where η_{spill}, η_{ph}, η_t, η_b, η_x, η_e and η_{et} are the efficiencies for spill-over, phase, taper, blockage, polarization, element and edge-taper, respectively. The η_o is the sum efficiencies of manufacturing accuracy, environmental factors, assembling errors and measurement mechanism. The η_{spill} is part of radiated power emanated at the feed on the RA aperture. The illumination efficiency (η_{ill}) is the product of η_t and η_{ph} as follows $\eta_{ill} = \eta_t \times \eta_{ph}$. The η_t and η_{ph} are the uniformity of amplitude

and phase distribution over the RA aperture. At design frequency, the phase error is almost zero once the element achieves complete phase range of 360˚. Therefore, some authors solely take into account η_t in η_{ill}. Among these sub-efficiencies, the product of η_{spill} and η_{ill} has the major effect on η_a. Finally, typical sub-efficiencies for RAs are tabulated in **Table 2** [7] [8] [9].

Element dimensions can be determined by the phase versus element change curve, when the necessary phase shift for each element is computed. However, element dimensions vary by a discrete value associated with the fabrication resolution, therefore, a sustained phase control is impossible. The discrepancy between desired element phase and quantized phase of the chosen element is classified as quantization-phase error. In this section, a study is undertaken to investigate the effects of quantization-phase errors on SLLs, HPBW and η_a. A broadside center-fed 30 cm square RA with sub-wavelength unit elements (lambda/3 at 10 GHz), $r_f = 1$, $q_f = 8.2$, and $q_e = 0.85$ is used in this study. The feed and element patterns are respectively modeled by the $\cos_f^{2q}(\theta_f)$ and $\cos_e^{2q}(\theta_e)$ due to its simplicity. **Figure 4** shows the phase distribution of the RA aperture at the ideal and various quantization phase, 45˚, 90˚ and 180˚ equal to 3-, 2- and 1-bit(s), respectively. **Figure 5** shows the radiation pattern which calculated by array-theory method [10].

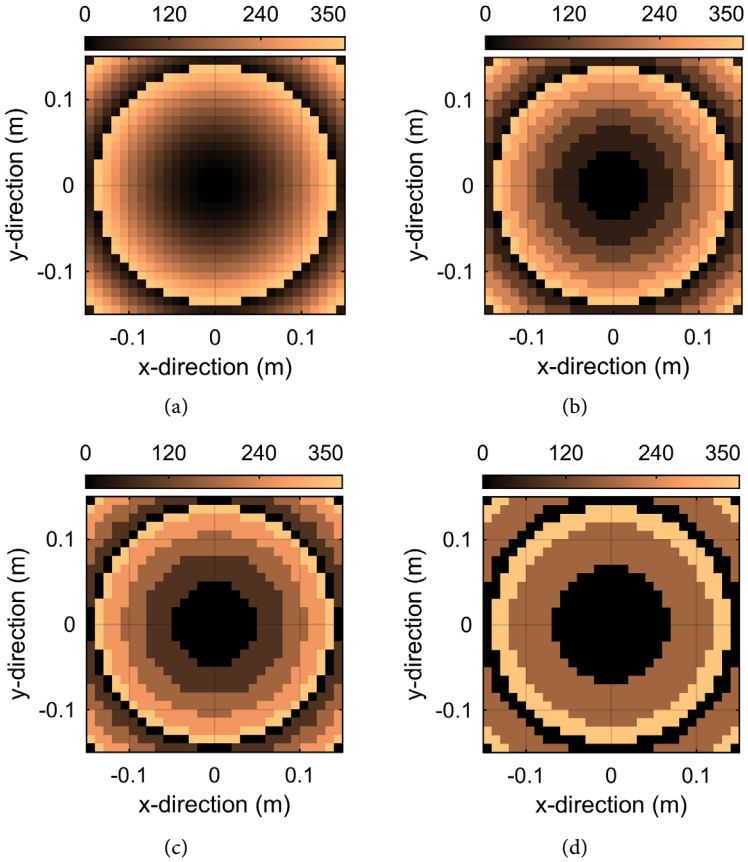

Figure 4. Phase distribution for different quantization-phase values. (a) 0˚; (b) 45˚; (c) 90˚; (d) 180˚.

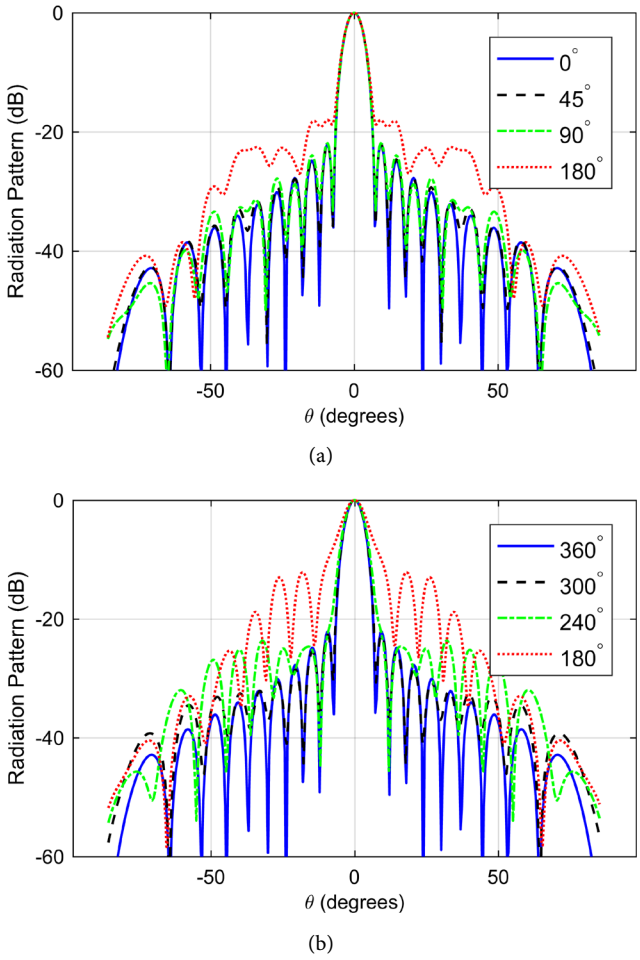

Figure 5. Radiation patterns for different values of: (a) quantization-phase; (b) phase-range.

Table 2. Typical sub-efficiencies for reflect array antennas.

Type of η	η (%)	Loss (dB)
η_{spill}	95	−0.22
η_{ill}	84	−0.76
η_f	96	−0.18
η_e	97	−0.13
η_x	95	−0.22
η_o	96	−0.18
η_a	68	−1.69

Sub-wavelength single resonance phasing elements have a phase-range below 360˚. So, some elements have unachievable phase shift. The radiation patterns for various element phase-ranges of 30 cm side-length square RA with $\theta_o = 0^\circ$, $\theta_b = 0^\circ$, $r_f = 1$, $q_f = 8.2$, and $q_e = 0.85$ are represented in **Figure 5(b)**. As can be observed from **Figure 5(a)** and **Figure 5(b)**, no grating lobe appears due to the

pseudo-random distribution of phase errors [11]. These effects are compared in Table 3 and Table 4. It is noticed that these errors increase SLLs, but have no major effects on the HPBW. Even the 45˚ quantization-phase or 180˚ phase-range cases has similar HPBW as RA with ideal phases. It can be a very helpful to cut back to the system complexity and cost, when the HPBW is a major demand.

A parametric study has been performed for center- and offset-fed square aperture RA, with side length 30 cm, $\lambda/3$ element spacing at 10 GHz, $q_e = 0.85$, $x_\circ = 0$ and $y_\circ = 0$, with different r_f, for each case q_f is considered to be maximum η_a. In this study, the offset-feed and main beam angles are equal. The η_a is derived from gain value [12], which includes η_{spill}, η_{ph} and η_t. In Figure 6, the acceptable quantization-phase without η_a reduction is around 30 and the threshold for phase-range is around 300˚. It shows reduction of η_a depends on quantization-phase or phase-range values, however, it is independent of offset-angle and feed location. The η_a reduction occurs when the SLLs is increased which in turn causes gain loss.

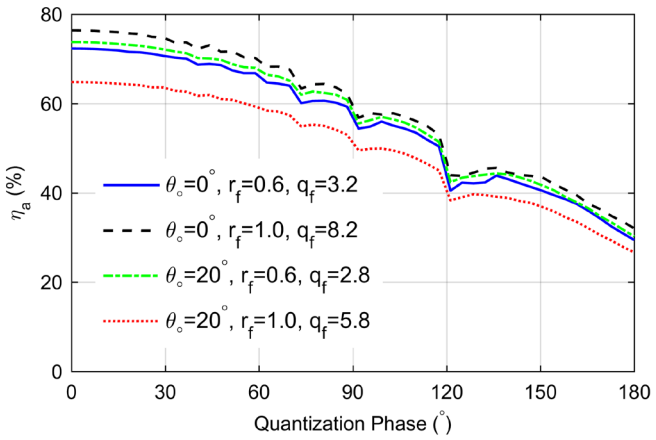

(a)

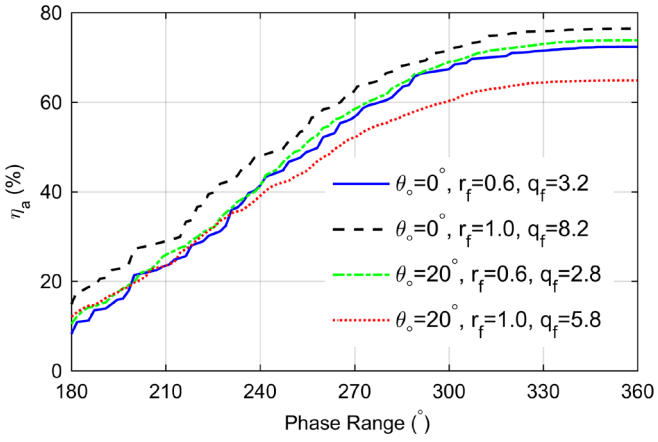

(b)

Figure 6. Reflect array antenna aperture efficiency versus. (a) Quantization-phase; (b) Phase-range.

Table 3. Effects of quantization-phase errors on reflect array antenna.

Quantization-Phase	0˚	45˚	90˚	180˚
Max. SLLs (dB)	−22.12	−22.04	−21.87	−18.00
HPBW (˚)	8.46	8.50	8.52	8.62
η_a (%)	76.39	72.70	59.50	32.06

Table 4. Effects of limited phase-range errors on reflect array antenna.

Phase-Range	360˚	300˚	240˚	180˚
Max. SLLs (dB)	−22.12	−22.65	−23.64	−12.13
HPBW (˚)	8.46	8.58	9.00	10.82
η_a (%)	76.39	71.47	47.97	14.85

3. Aperture Efficiency Study

Parameters of square aperture RA with a side length of $10\lambda_0$ (λ_0 is lambda at 10 GHz) are studied. Two designs with a $\theta_o = 0^\circ$, $q_f = 8.2$; and $\theta_o = 20^\circ$, $q_f = 2.8$ are considered, other parameters are: $x_o = 0$, $y_o = 0$, and $q_e = 0.85$. η_{spill}, η_{ill} and $\eta_a = \eta_{spill} \times \eta_{ill}$ are plotted in **Figure 7** and as shown the maximum accessible η_a value for center-fed (76.44%) is greater than offset-fed (62.58%). Also, in **Figure 7** as r_f grows the η_{spill} decreases due to a bigger r_f reduced aperture angle of the RA plane with respect to the feed source. In addition, η_{ill} increases since it forms a more uniform field distribution on the array.

For a precise design, the effects of excitation angle (θ_{inc}, φ_{inc}) for each element ought to be considered. **Figure 8** displays the range and distribution of plane wave excitation angles in the RA aperture. It can be observed that the upper part of the RA aperture has a maximum θ_{inc}. So, the element spacing should have selected small enough that no distributed grating lobe radiated [1]. Comparison of **Figure 8(a)** and **Figure 8(b)** indicates that the percentage of aperture area illuminated with incident angle larger than 30˚ in the central case is less than 5.6% whereas in offset-feed RA is about 66.7%. Therefore, the impact of incidence angle is anticipated to be more significant in offset fed RAs. So, the use of sub-wavelength element appears to be necessary [13]. In the RA design process, an excitation plane wave can always be decomposed into a combination of the zero TE- and TM-waves [1]. In [14], it is indicated that magnitude of reflection components depends on both the θ_{inc} and φ_{inc}, and it ought to be considered for every element.

The feed position is determined by offset angle (θ_o) and the distance r_f. **Figure 9(a)** and **Figure 9(b)** show the η_a versus r_f and q_f with other parameters set as: $x_o = 0$, $y_o = 0$, and $q_e = 0.85$. In **Figure 9(a)**, in center-fed case for every r_f it is possible to find a q_f that maximize η_a. However, in offset-fed RA, the maximum of η_a is obtained just for lower r_f and q_f values, as presented in **Figure 9(b)**. In **Figure 9(a)**, an η_a around 70% is realized for various mixtures of r_f and q_f, however for larger r_f and q_f a wider bandwidth can be achieved [12]. Since the feed is

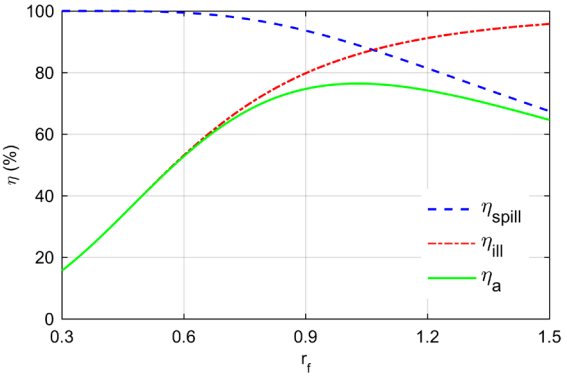

(a)

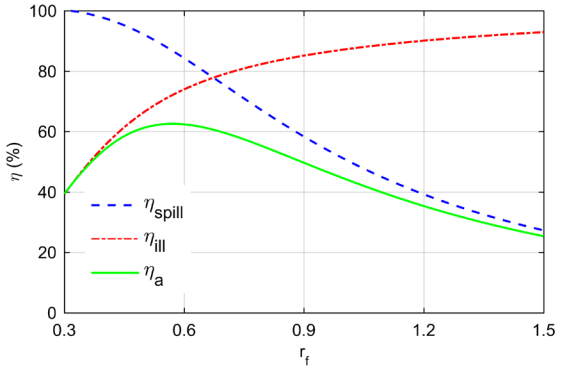

(b)

Figure 7. η_{ill}, η_{spill}, and η_a for square aperture. (a) $\theta_o = 0^\circ$, $q_f = 8.2$; (b) $\theta_o = 20^\circ$, $q_f = 2.8$.

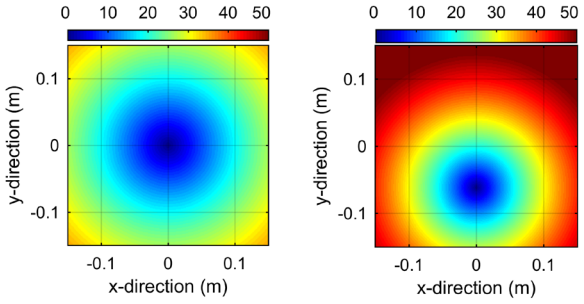

(a)

(b)

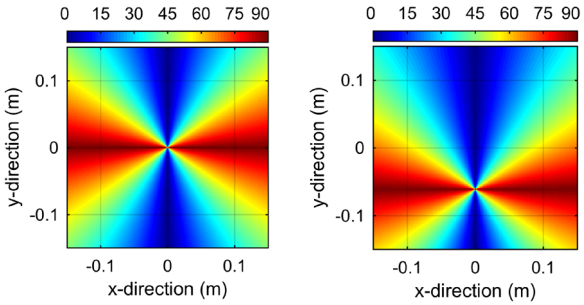

(c)

(d)

Figure 8. Excitation angles distribution on the RA aperture θ_{inc} for (a) $\theta_o = 0^\circ$, $r_f = 1$; (b) $\theta_o = 20^\circ$, $r_f = 0.6$; φ_{inc} with mapping into the 0° - 90° for (c) $\theta_o = 0^\circ$, $r_f = 1$; (d) $\theta_o = 20^\circ$, $r_f = 0.6$.

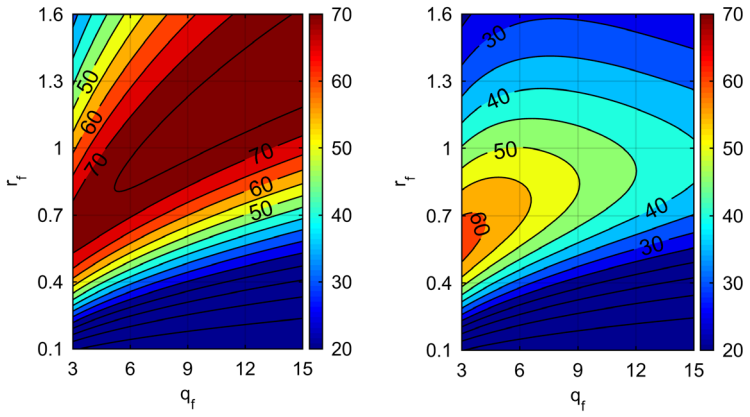

Figure 9. The η_a for square aperture versus both q_f and r_f (a) $\theta_o = 0^\circ$; (b) $\theta_o = 20^\circ$.

placed in y-z plane, the plane of incidence, it is proper to use the coordinate (y_f, z_f) for parametric study. The results are displayed in **Figure 10(a)** and **Figure 10(b)** for $q_f = 2.8$ and $q_f = 8.2$, respectively, other fixed parameters are: $x_o = 0$, $y_o = 0$, and $q_e = 0.85$. It is noted that once $q_f = 2.8$, η_a is varied from 60% to 70%, and when $q_f = 8.2$, the maximum η_a is achieved at higher feed position. Larger q_f value yields a narrower feeding beam width. So, a larger r_f ought to have an additional uniform field distribution on the aperture. Using this contour map, one might find a correct feed location. The maximum η_a is acquired close to $z_f = 290$ mm, as determined in **Figure 10(b)**. The η_a keeps nearly constant until y_f is shifted to -50mm with z_f fixed in 297 mm.

The contoured η_a plot versus x_o and y_o are depicted in **Figure 11**, with the fixed parameters: $r_f = 1.0$, $\theta_o = 0^\circ$, $q_f = 8.2$, and $q_e = 0.85$ for center-fed; $r_f = 0.6$, $\theta_o = 20^\circ$, $q_f = 2.8$, and $q_e = 0.85$ for offset-fed RA. It is noted that for offset case maximum efficiency is obtained once the feeding beam is pointed at 13 mm away from aperture center, when η_a reaches 63%. Besides, the symmetry of the η_a with respect to x-axis is observed. In most RAs $x_o = 0$, and $y_o = 0$, therefore center elements have a stronger illumination and contribute more to total radiation. Accordingly, the useful information of an RA performance can be deduced without simulating whole structure. For example, a decent approximation of the RA gain bandwidth can be estimated by calculating the scattering from the middle row of a large RA enclosed by perfectly magnetic conductor (PMC) boundaries [15]. For gain bandwidth enhancement, one might place elements with smaller reflection loss at the central area of the aperture. This can be done by adding a phase constant to the phase distribution over the RA aperture. Considering both q_f and q_e results a contour plot of η_a in **Figure 12** with constant parameters: $r_f = 1.0$, $\theta_o = 0^\circ$, $x_o = 0$, and $y_o = 0$ for center-fed; $r_f = 0.6$, $\theta_o = 20^\circ$, $x_o = 0$, and $y_o = 0$ for offset-fed. Note that the parameters q_e solely effects η_{ill}. **Figure 12(a)** and **Figure 12(b)** show the fact that the q_e plays a smaller role in the η_a than q_f.

Finally, effects of configuration parameters are studied separately. **Figure 13(a)**

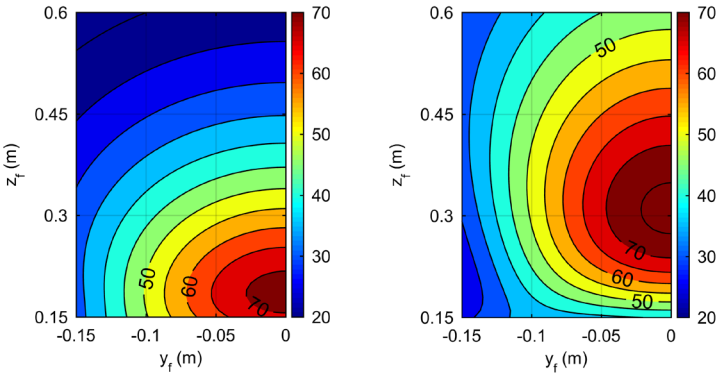

Figure 10. The η_a versus feed location in y-z plane. (a) $q_f = 2.8$; (b) $q_f = 8.2$.

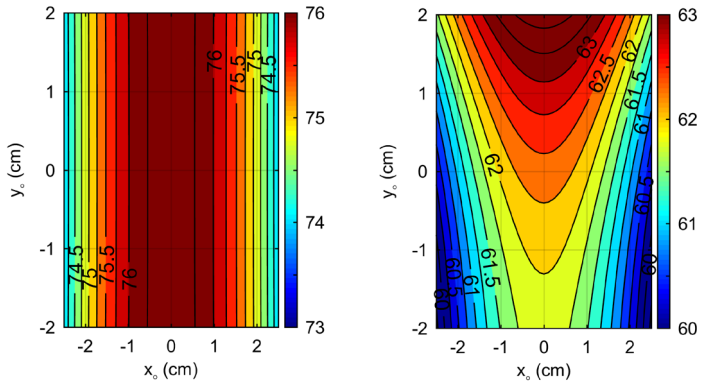

Figure 11. The η_a versus feed orientation $P_o(x_o, y_o, 0)$. (a) Center-fed; (b) Offset-fed.

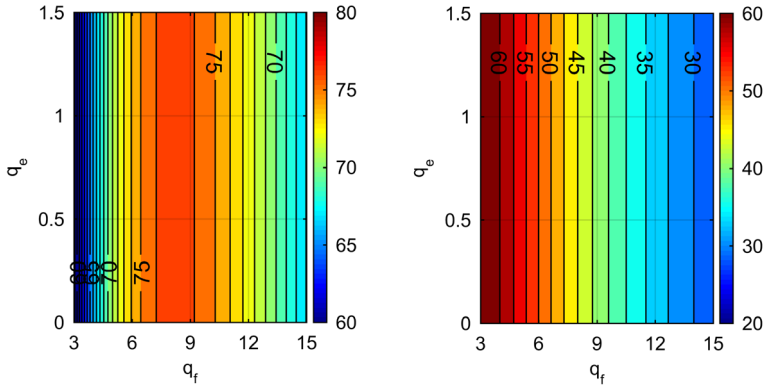

Figure 12. The aperture efficiency versus both q_f and q_e. (a) Center-fed; (b) Offset-fed.

demonstrates the maximum η_a at $r_f = 1.02$ once the feed has $\theta_o = 0^\circ$ and $q_f = 8.2$. Comparison of center- and offset-cases shows the importance of right selection of RA parameters. Selecting an incorrect q_f and r_f for a given RA leads to a considerably low η_a. Another curve, shown in **Figure 13(b)**, provides η_a as a function of θ_o. The maximum η_a appears at the center feed position ($\theta_o = 0^\circ$) and

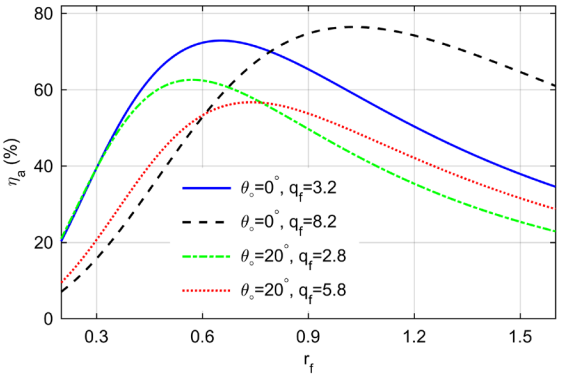

(a)

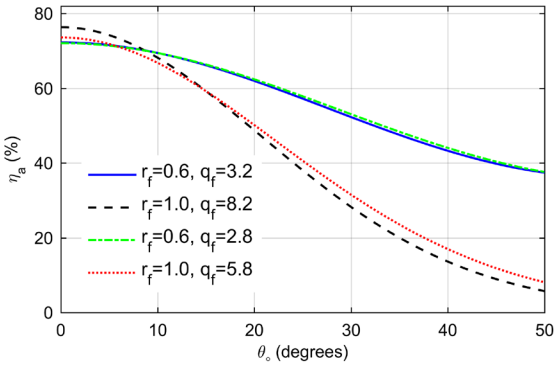

(b)

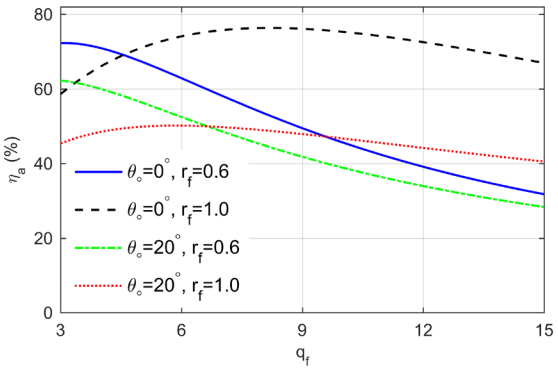

(c)

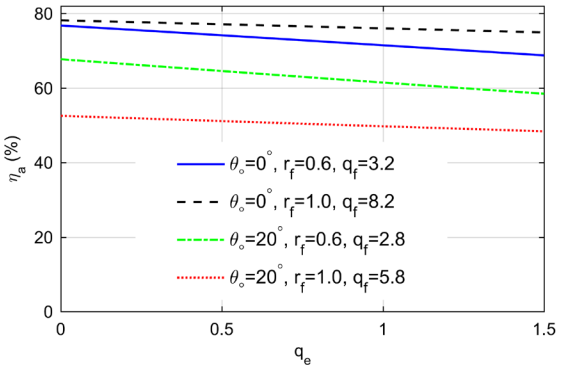

(d)

Figure 13. The aperture efficiency versus. (a) r_f; (b) $\theta_\circ$; (c) q_f; (d) q_e.

maintains a certain offset angle depending on r_f and q_f values. For RAs with higher r_f and q_f this offset-angle is around 10˚ and experience shows a maximum of 15˚ offset-angle is allowed for acceptable η_a. The curve of feed pattern function is described in **Figure 13(c)**. The optimum q_f for center-fed case with r_f = 0.6 is 3.2 and 6.3 for the 20˚ offset-fed RA with r_f = 1.0. The variation of q_f to obtain a maximum η_a between center- and offset-fed for r_f = 0.6 is smaller amount than r_f = 1.0. Likewise, the curve of the η_a versus q_e is depicted in **Figure 13(d)**. RAs with smaller r_f and offset-fed location, the η_a is further attenuated by the element pattern.

4. Conclusion

The quantization-phase and limited phase-range errors reduce RA antenna efficiency and increase SLLs, however, the HPBW remains mostly constant. The maximum acceptable quantized phase with negligible η_a diminution is around 30˚ and this threshold for limited phase-range is near 300˚. The limitations are independent of offset angle and feed location. Based on conducted parametric studies for a square aperture RA with side length 30 cm, it was observed that the appropriate selection of r_f and q_f has a significant effect on η_a and a center-fed RA has the maximum η_a. However, the η_a preserves its behavior up to 15˚ for offset-fed with smaller r_f and q_f.

References

[1] Huang, J. and Encinar, J.A. (2008) Reflect Array Antennas, John Wiley & Sons, Hoboken.

[2] Shaker, J., Chaharmir, M.R. and Ethier, J. (2013) Reflect Array Antennas, Analysis, Design, Fabrication, and Measurement. Artech House, Norwood, Massachusetts.

[3] Nayeri, P., Yang, F. and Elsherbeni, A.Z. (2018) Reflect Array Antennas: Theory, Designs, and Applications. John Wiley & Sons, Hoboken. https://doi.org/10.1002/9781118846728

[4] Xu, S. and Yang, F. (2015) Handbook of Antenna Technologies: Reflect Array Antennas. Springer, Berlin.

[5] Poghosyan, A. and Golkar, A. (2017) CubeSat Evolution: Analyzing CubeSat Capabilities for Conducting Science Missions. *Progress in Aerospace Sciences*, **88**, 59-83. https://doi.org/10.1016/j.paerosci.2016.11.002

[6] Hodges, R.E., Chahat, N., Hoppe, D.J. and Vacchione, J.D. (2017) A Deployable High-Gain Antenna Bound for Mars: Developing a New Folded-Panel Reflect Array for the First CubeSat Mission to Mars. *IEEE Antennas and Propagation Magazine*, **59**, 39-49. https://doi.org/10.1109/MAP.2017.2655561

[7] Yu, A., Yang, F., Elsherbeni, A.Z., Huang, J. and Samii, Y.R. (2012) Aperture Efficiency of Reflect Array Antennas. *Microwave and Optical Technology Letters*, **52**, 367-368. https://doi.org/10.1002/mop.24949

[8] Huang, J. (1995) Analysis of Microstrip Reflect Array Antenna for Microspacecraft Applications. *TDA Progress Report*, **42-120**, 158-160.

[9] Pozar, D.M., Targonski, S.D. and Syrigos, H.D. (1997) Design of Millimeter-Wave Microstrip Reflect Arrays. *IEEE Transactions on Antennas and Propagation*, **45**,

287-296. https://doi.org/10.1109/8.560348

[10] Nayeri, P., Elsherbeni, A.Z. and Yang, F. (2013) Radiation Analysis Approaches for Reflect Array Antennas. *IEEE Antennas and Propagation Magazine*, **55**, 127-134. https://doi.org/10.1109/MAP.2013.6474499

[11] Yang, H., Yang, F., Xu, S., Li, M., Cao, X., Gao, J. and Zheng, Y. (2017) A Study of Phase Quantization Effects for Reconfigurable Reflect Array Antennas. *IEEE Antennas and Wireless Propagation Letters*, **16**, 302-305. https://doi.org/10.1109/LAWP.2016.2574118

[12] Devireddy, B., Yu, A., Yang, F. and Elsherbeni, A.Z. (2011) Gain and Bandwidth Limitations of Reflect Arrays. *Applied Computational Electromagnetics Society Journal*, **26**, 170-178.

[13] E'qab, R.F. and McNamara, D.A. (2016) Angle of Incidence Effects in Reflect Array Antenna Design: Making Gain Increases Possible by Including Incidence Angle Effects. *IEEE Antennas and Propagation Magazine*, **58**, 52-64. https://doi.org/10.1109/MAP.2016.2594699

[14] Fujii, Y., Yoshimoto, S., Makino, S., Hirota, T., Noguchi, K. and Itoh, K. (2015) The Design Method of Low-Cross-Polarization Reflect Array Antenna. *IEEE* 2015 *International Symposium in Antennas and Propagation* (*ISAP*), Hobart, TAS, 9-12 November 2015, 765-767.

[15] Chaharmir, M.R., Shaker, J., Gagnon, N. and Lee, D. (2010) Design of Broadband, Single Layer Dual-Band Large Reflect Array Using Multi Open Loop Elements. *IEEE Transactions on Antennas and Propagation*, **58**, 2875-2883. https://doi.org/10.1109/TAP.2010.2052568